The electronic structure of the novel rare-earth permanent magnet $Sm_2Fe_{17}N_3$

1993 J. Phys.: Condens. Matter 5 6911

(http://iopscience.iop.org/0953-8984/5/37/009)

J. Phys.: Condens. Matter 5 (1993) 6911–6924. Printed in the UK

The electronic structure of the novel rare-earth permanent magnet $Sm_2Fe_{17}N_3$

B I Min†, J-S Kang‡, J H Hong‡, S W Jung‡, J I Jeong‡, Y P Lee‡, S D Choi‡, W Y Lee‡, C J Yang‡ and C G Olson§

† Department of Physics, Pohang Institute of Science and Technology, Pohang 790-600, Korea
‡ Research Institute of Industrial Science and Technology, Pohang 790-600, Korea
§ Ames Laboratory, Iowa State University, Ames, IA 50011, USA

Received 5 May 1993, in final form 14 July 1993

Abstract. Electronic and magnetic properties of the novel rare-earth permanent magnet $Sm_2Fe_{17}N_3$ are investigated by performing self-consistent local density-functional electronic-structure calculations. We also report valence-band photoemission studies on Sm_2Fe_{17}, which is the matrix compound of $Sm_2Fe_{17}N_3$, and on Nd_2Fe_{17} for comparison. Employing the LMTO (linearized muffin-tin orbital) band method, we have obtained electronic band structures for both paramagnetic and ferromagnetic phases of $Sm_2Fe_{17}N_3$, Sm_2Fe_{17}, and Nd_2Fe_{17}. It is found that N atoms substantially reduce the magnetic moment of neighbouring Fe atoms through the hybridization interaction and play a role in stabilizing the structure. The average magnetic moment of Fe atoms in the ferromagnetic phase of $Sm_2Fe_{17}N_3$ is estimated to be $2.29\mu_B$, which is $\sim 6\%$ larger than the magnetic moment of Sm_2Fe_{17}, $2.16\mu_B$. Photoemission spectroscopy (PES) measurements show that the *bulk* Nd and Sm atoms are nearly trivalent in Nd_2Fe_{17} and Sm_2Fe_{17}, and that broad 4f PES line shapes reflect the hybridization between Nd/Sm 4f and Fe 3d states. The experimental Fe 3d PES spectra are compared with the calculated Fe 3d angular-momentum-projected local density of states (PLDOS) for Nd_2Fe_{17} and Sm_2Fe_{17}. The measured Fe 3d PES band widths are comparable to the calculated Fe 3d PLDOS widths below E_F, but the peak positions lie in between the calculated peaks of the paramagnetic and ferromagnetic Fe 3d PLDOS.

1. Introduction

R_2Fe_{17} compounds have attracted much attention as candidates for possible new permanent-magnet materials, because they have the largest Fe concentration among the intermetallic compounds of rare earths (R) and transition metals (M), and so very large magnetic moments. R_2Fe_{17} compounds, however, have low Curie temperatures T_C and low anisotropy fields H_a, which prohibit them from being used as permanent magnetic materials. Recently, Coey *et al* [1] discovered that adding the element N into R_2Fe_{17} yields $R_2Fe_{17}N_{3-\delta}$, which show several promising features such as high T_C, increased by $\sim$ 400 K, and enhanced H_a, as compared to R_2Fe_{17}.

The crystal structure of R_2Fe_{17} is maintained in $R_2Fe_{17}N_{3-\delta}$, with the volume increased slightly (by $\sim$ 6%). $R_2Fe_{17}N_{3-\delta}$ compounds crystallize in the rhombohedral Th_2Zn_{17}-type structure for light rare earths (R from La to Tb), whereas for heavy rare earths (R from Dy to Lu), and for $Y_2Fe_{17}N_{3-\delta}$, they crystallize in the hexagonal Th_2Ni_{17}-type structure. In particular, it is very encouraging that the axial anisotropy along the c axis is observed in $Sm_2Fe_{17}N_{3-\delta}$, in contrast to other $R_2Fe_{17}N_{3-\delta}$ compounds, which exhibit planar anisotropy. Compared to the existing rare-earth permanent-magnet materials, such

0953-8984/93/376911+14$07.50

as $SmCo_5$ and $Nd_2Fe_{14}B$, $Sm_2Fe_{17}N_{3-\delta}$ shows overall advantages in the magnetic properties of T_C, H_a, and saturated magnetization B_S [2–5].

On the electronic structure of $Sm_2Fe_{17}N_3$, Woods *et al* [6] have reported preliminary results, obtained by photoemission spectroscopy (PES) measurements and by self-consistent band-structure calculations. Without showing the measured PES data, they reported that, as compared to Sm_2Fe_{17}, a small shift of the Fe 3d band to higher binding energy and a reduction of the density of states (DOS) at the Fermi energy E_F, are observed in $Sm_2Fe_{17}N_3$, which is in agreement with the band theory. No other studies have been reported yet, either theoretically or experimentally. For related materials, several theoretical studies have been reported such as band-structure calculations on $Y_2Fe_{17}N_3$ by Jaswal *et al* [7], using the self-consistent LMTO (linearized muffin-tin orbital) method [8], and those on $Nd_2Fe_{17}N_3$ by Gu and Lai [9], using the OLCAO (orthogonalized linear combination of atomic orbitals) band method. Unfortunately, $Y_2Fe_{17}N_3$, investigated by Jaswal *et al*, has a crystal structure, i.e., the hexagonal Th_2Ni_{17} type, different from that of $Sm_2Fe_{17}N_3$. On the other hand, $Nd_2Fe_{17}N_3$ has the same crystal structure as that of $Sm_2Fe_{17}N_3$, i.e., the rhombohedral Th_2Zn_{17} type, but the OLCAO band results of Gu and Lai were not obtained self-consistently.

In this paper, we report electronic-structure studies of $Sm_2Fe_{17}N_{3-\delta}$, as well as photoemission measurements and band-structure calculations for R_2Fe_{17} (R=Nd, Sm). We have performed both spin-unpolarized and spin-polarized calculations, in which the von Barth–Hedin formula is used for the exchange–correlation interaction in the local density-functional approximation (LDA) method [10]. Energy band structures and DOS are obtained by using the self-consistent semi-relativistic LMTO band method and a Gaussian broadening method [11], respectively. The orbital contribution to the magnetic moment is calculated by considering the spin–orbit interaction in a perturbative way [12]. The valence-band PES spectra of R 4f and Fe 3d electrons are obtained by using synchrotron-radiation PES. Measured PES spectra are compared to the calculated band structures.

2. Electronic structures of $Sm_2Fe_{17}N_3$

2.1. Crystal structure

Figure 1 shows the crystal structure of $Sm_2Fe_{17}N_3$: the rhombohedral Th_2Zn_{17}-type structure (belonging to the D^5_{3d} space group), in which three N atoms are added into interstitial sites of Sm_2Fe_{17}. There are 22 atoms per unit cell and thus one formula unit in the rhombohedral unit cell; two Sm atoms of one kind, 17 Fe atoms of four kinds, and three N atoms of one kind. It is interesting that many crystallographic parallels exist between Sm_2Fe_{17}, the matrix of $Sm_2Fe_{17}N_3$, and $Nd_2Fe_{14}B$, which is one of the typical rare-earth permanent magnets, such as the layered arrangement and the presence of hexagonal Fe nets surrounding R atoms. A unit cell consists of a stack of six layered planes, and Sm atoms reside in three planes among them while three other intervening planes are made of Fe atoms only. FeIII(18f) atoms surround Sm atoms in hexagonal nets, residing in the same plane as Sm atoms. The FeII(9d) and FeIV(18h) atoms also form hexagonal nets in the intervening planes.

It is notable that the local environment of FeI(6c) atoms in Sm_2Fe_{17} is crystallographically very similar to that of Fe(j_2) atoms in $Nd_2Fe_{14}B$ [4]. The layers of Fe(j_2) atoms in $Nd_2Fe_{14}B$ are midway between the planes containing Nd and B atoms, and they have the largest magnetic moment. Similarly in Sm_2Fe_{17}, a pair of dumbbell-like FeI(6c) atoms, located above and below the centres of the FeIII(18f) hexagons, connect all of the layered planes (see figure 1). They have the largest number of near-neighbour Fe atoms and so are expected to have the largest magnetic moment in the ferromagnetic phase.

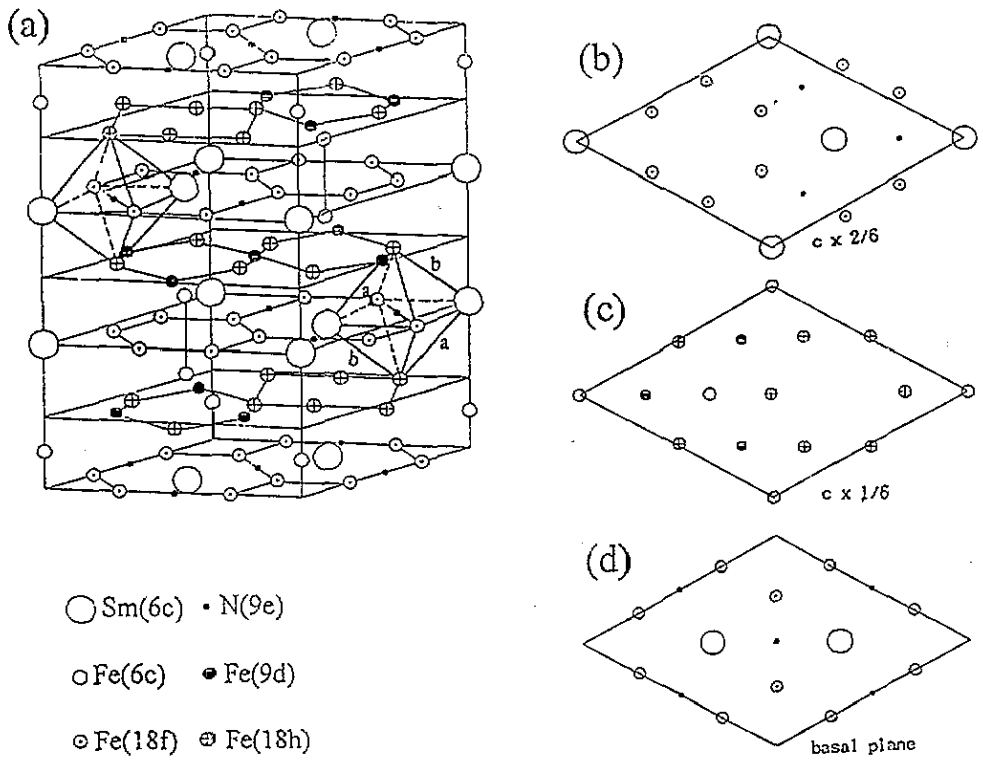

Figure 1. Crystal structure of $Sm_2Fe_{17}N_3$ (rhombohedral Th_2Zn_{17}-type structure).

In $Sm_2Fe_{17}N_3$, N atoms are added to Sm_2Fe_{17} at the (9e) octahedral sites surrounded by Sm and FeIII(18f) atoms in the plane and by FeIV(18h) atoms along the z direction. Three N atoms are inserted in the middle of the three bonds among the six FeIII(18f) hexagon bonds, and therefore the bond length of FeIII–N–FeIII becomes larger than that of FeIII–FeIII, yielding a distorted hexagon surrounding Sm atoms in $Sm_2Fe_{17}N_3$.

2.2. Computational details

The crystal structure of $Sm_2Fe_{17}N_3$ is not so close packed as that of $Sm_2Fe_{17}N_3$, with a packing ratio of about 55%. Our experience is that the atomic sphere approximation (ASA) works well for materials with such packing ratios, and so we have used the LMTO ASA in our calculation without using empty spheres. The atomic-sphere radii utilized are 3.82, 2.66, and 1.73 au for Sm, Fe, and N atoms, respectively.

It is a well known fact that, in any material with localized f electrons, is very difficult to obtain self-consistent convergency in a band-structure calculation. In our calculation, we have used Broyden's accelerating mixing scheme [13] with a very small mixing parameter, 0.01. Self-consistent charge densities are obtained by using one $\boldsymbol{k}$ point for the Brillouin-zone integration, which saves much time despite the many iterations necessary. Final results are obtained by using twelve $\boldsymbol{k}$ points inside an irreducible Brillouin zone. Due to the large unit cell of $Sm_2Fe_{17}N_3$, this procedure is expected to give reasonable results.

We have used a semi-relativistic band method in self-consistent calculations, which includes all the relativistic effects except the spin–orbit effect. The effect of spin–orbit

interaction is then taken into account in a perturbative way to calculate the orbital magnetic moment of each atom [12].

We have calculated band structures for the cases with the Sm 4f electrons as core and also as valence electrons. When treating 4f electrons as core electrons, the 4f shell is considered to remain in its ionic ground-state trivalent configuration, with five f electrons fully spin polarized. This is the so called *open-4f-core-shell* method often employed to treat localized f electrons [4]. We have utilized this treatment to obtain the 4f removal energy through the *delta-self-consistent field* (ΔSCF) total-energy calculation [15].

2.3. *Spin-unpolarized calculation*

Figure 2(a) shows the total density of states for the paramagnetic $Sm_2Fe_{17}N_3$, calculated at experimental lattice constants by treating Sm f electrons as valence electrons. The advantage of treating Sm f electrons as valence electrons and including them in the self-consistent calculations is that magnetic properties of the Sm f electrons can be described more appropriately. The total DOS shows two pronounced peaks near E_F. The left peak is mostly due to the Fe d-band states and the right one is due to the Fe d and Sm f states. The DOS $N(E_F)$ at E_F is very large in the paramagnetic phase of $Sm_2Fe_{17}N_3$. The Stoner factor, defined as $S \equiv N(E_F)I_{XC}$ with I_{XC} denoting the intra-atomic exchange–correlation integral, becomes larger than one ($S = 2.7$) because of the high DOS at E_F, and so ferromagnetic instability occurs.

Table 1 presents the angular-momentum-projected charge occupancies Q_l in the paramagnetic phase of $Sm_2Fe_{17}N_3$. The number of 4f electrons per Sm atom is about 6.20, while the number of 3d electrons per Fe atom ranges from approximately 6.5 to 6.7, which is close to the value of the pure BCC Fe element, ~ 6.6. It is seen that there occurs a charge transfer to the FeIII atom from neighbouring atoms, especially from near-neighbour N atoms.

Table 1. Angular-momentum-projected charge occupancies Q_l of paramagnetic $Sm_2Fe_{17}N_3$. The atomic-sphere radii for Sm, Fe, and N atoms are 3.82, 2.66, and 1.73 au, respectively.

	Q_s	Q_p	Q_d	Q_f	Q_{tot}
Sm	0.57	1.00	1.93	6.17	9.67
FeI	0.64	0.66	6.47	—	7.75
FeII	0.66	0.77	6.56	—	7.99
FeIII	0.62	0.84	6.66	—	8.12
FeIV	0.61	0.71	6.55	—	7.87
N	1.20	2.88	—	—	4.08

Figure 2(b) shows the projected local density of states (PLDOS) for $Sm_2Fe_{17}N_3$. The sharp narrow peak near E_F represents the Sm 4f LDOS, and the four bands on the left side, which overlap one another, represent Fe 3d bands. Among Fe atoms, FeI and FeIII atoms have the highest and the lowest LDOS, respectively, at E_F. These Fe 3d band structures are quite different from those of Sm_2Fe_{17}, in that the magnitudes of the FeIII LDOS and the FeI LDOS at E_F are similar in Sm_2Fe_{17} [16]. The FeIII LDOS at E_F is smaller in $Sm_2Fe_{17}N_3$ than in Sm_2Fe_{17}, which reflects hybridization effects between FeIII atoms and near-neighbour N atoms in $Sm_2Fe_{17}N_3$. Remember that FeIII and N atoms reside in the same plane, and thus a large hybridization between them is expected. The N p bands spread between -8 eV and 8 eV, and are split into the bonding and anti-bonding states due to the hybridization interaction with the Sm 5d, FeIII, and FeIV 3d states. This feature indicates that N atoms

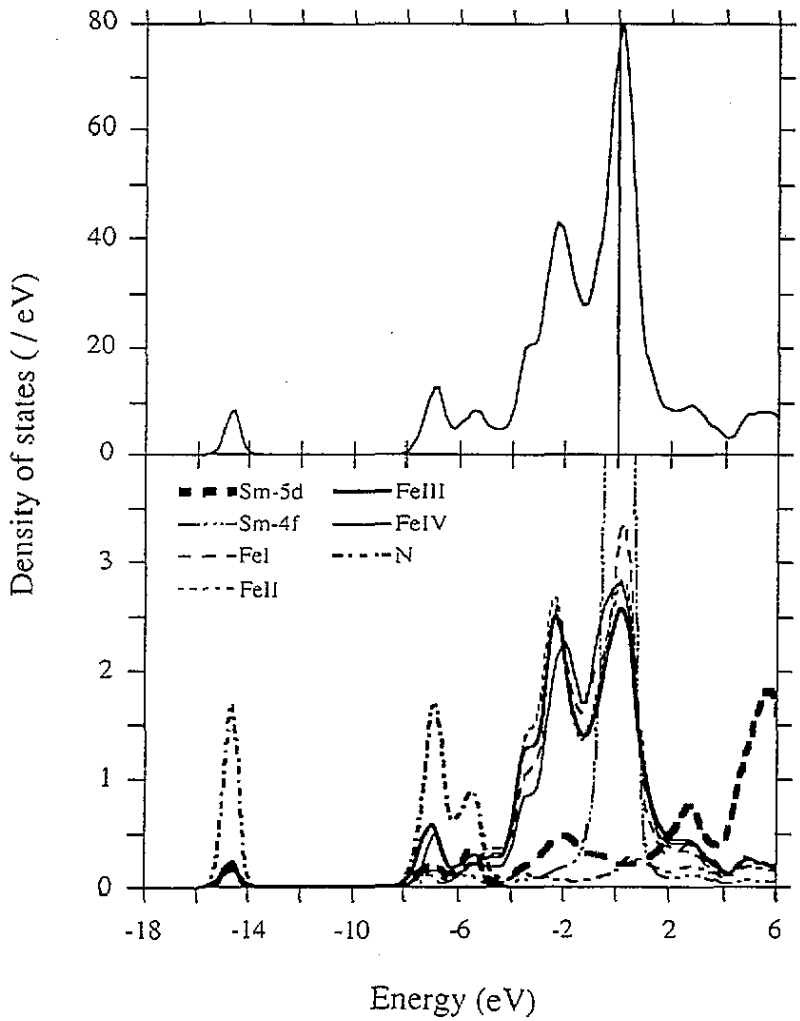

Figure 2. (a) Total density of states (DOS) of paramagnetic $Sm_2Fe_{17}N_3$. (b) Site- and angular-momentum-projected local density of states (PLDOS) of each atom in the paramagnetic $Sm_2Fe_{17}N_3$.

in $Sm_2Fe_{17}N_3$ play the role of lowering $N(E_F)$ so as to contribute to the structural stability via the hybridization bonding with the Sm d, f, and Fe 3d states. The role of N atoms in $Sm_2Fe_{17}N_3$ is similar to that of B atoms in $Nd_2Fe_{14}B$ [17].

Rather low and localized LDOS around 15 eV below E_F mainly corresponds to the N s bands, in which s and d bands of FeIII atoms and d and f bands of Sm atoms are mixed. As mentioned above, the hybridization interaction of the N s bands with the FeIII 3d bands is particularly large. The binding energy of N s states ($\sim$ 15 eV) in $Sm_2Fe_{17}N_3$ is larger than that of B s states ($\sim$ 8 eV) in $Nd_2Fe_{14}B$ by about 7 eV. This difference is consistent with the trend that binding energies of s states in YCo_4X increase as 9, 11, 15, and 18 eV for X = B, C, N, and O, respectively [16]. However, we have found that binding energies of the s states are sensitive to the atomic-sphere radii of N atoms used in LMTO calculations. When we used larger atomic-sphere radii for N atoms (2.02 au), the energy position of N

s states becomes unphysically too low (~ -29 eV), which is ascribed to large overlaps of atomic spheres. Magnetic moments of Fe atoms are also dependent on the size of atomic spheres, a maximum of $\sim 5\%$ change with 1% increase in Fe atomic-sphere radii. In this study, we have chosen atomic-sphere radii of N atoms so that the energy position of N s states is consistent with those of YCo_4X [16], and those of Fe atoms to be nearly equal to that of the BCC Fe element. The LDOS in figure 2(b) is obtained by using 1.73 and 2.66 au for the atomic-sphere radii of N and Fe atoms, respectively.

2.4. *Spin-polarized calculation*

Figure 3(a) shows the spin-polarized DOS for $Sm_2Fe_{17}N_3$ in the ferromagnetic phase. In our calculation, we have assumed a single quantization axis and the moments are forced to line up parallel or antiparallel to it. The DOS in the paramagnetic phase is split into the spin-up and spin-down DOS due to the exchange–correlation band splitting, so that the DOS at E_F is reduced by about a half ($N(E_F) = 32.6$ states eV^{-1}/cell). In contrast to the paramagnetic phase, the spin-up DOS at E_F is mostly due to Sm 4f states and the spin-down DOS to Fe 3d states, because Fe 3d spin-up band states are almost filled and Sm 4f spin-down states are located far above E_F due to the band splitting. Note that the above energy position of Sm 4f spin-up states does not agree with the energy position of localized 4f electrons observed in the PES data, as will be shown in figure 4(b). This is because the PES data are excited-state properties, while the LDA band results are for the ground-state properties. The so-called Δ SCF supercell calculation is required to obtain the excitation energy of the localized f electrons. Our Δ SCF calculation yields the 4f removal energy ($f^5 \rightarrow f^4$) in $Sm_2Fe_{17}N_3$ of ~ 6.9 eV, which is in reasonably good agreement with the PES data discussed in section 3.

Table 2 shows the angular-momentum-projected magnetic moments M_l in the ferromagnetic phase of $Sm_2Fe_{17}N_3$. The spin magnetic moment of Sm 4f electrons is $5.46\mu_B$, and the total spin magnetic moment at the Sm site is $5.31\mu_B$. Similarly, the spin magnetic moments at four kinds of Fe atomic site are 2.65, 2.46, 1.96, and $2.42\mu_B$, respectively, yielding the average spin magnetic moment per Fe atom of $2.29\mu_B$. Compared to the spin magnetic moment of the BCC Fe metal ($2.22\mu_B$), the spin magnetic moment at the FeIII atomic site is reduced, whereas those at the other Fe sites are very much enhanced. The spin magnetic moments of N atoms are negligible. When the spin magnetic moments of Sm 4f electrons are included, the total spin magnetic moment M_{tot} per unit cell is $49.46\mu_B$ for $Sm_2Fe_{17}N_3$. When the Sm 4f electrons are treated as core electrons, we have obtained $M_{tot} = 39.63\mu_B$, the magnitude of which is similar to that for $Y_2Fe_{17}N_3$, the *non*-f-electron material, calculated by Jaswal *et al* [7] ($39.60\mu_B$).

Table 2. Angular-momentum-projected magnetic moments M_l of ferromagnetic $Sm_2Fe_{17}N_3$.

	M_s	M_p	M_d	M_f	M_{tot}
Sm	−0.02	−0.05	−0.08	5.46	5.31
FeI	−0.01	−0.06	2.72	—	2.65
FeII	−0.02	−0.06	2.54	—	2.46
FeIII	−0.02	−0.06	2.03	—	1.96
FeIV	−0.02	−0.05	2.47	—	2.42
N	−0.02	−0.02	—	—	−0.04

As has been expected in the paramagnetic electronic structure, FeIII atoms have the smallest spin magnetic moment, $1.96\mu_B$, which is due to the hybridization interaction with

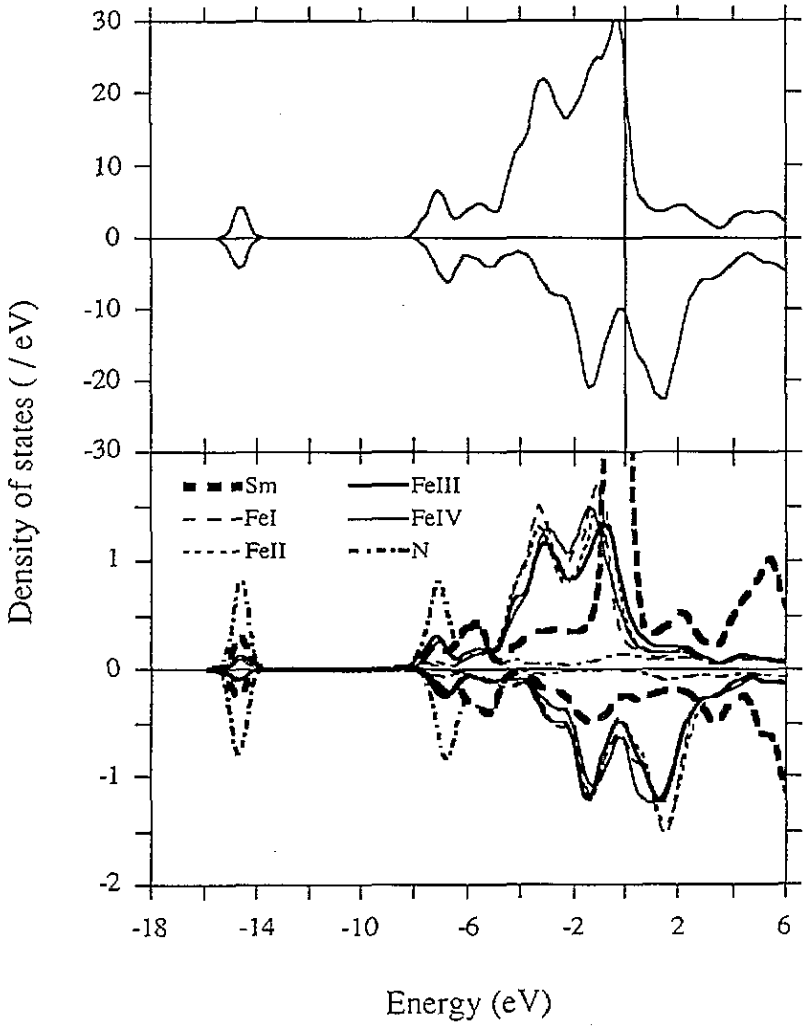

Figure 3. (a) Total density of states (DOS) of ferromagnetic $Sm_2Fe_{17}N_3$. The upper and lower curves correspond to spin-up and spin-down DOS, respectively. (b) Site- and angular-momentum-projected local density of states (PLDOS) of each atom in the ferromagnetic $Sm_2Fe_{17}N_3$.

N atoms and to the local environment. This finding is consistent with that of Gu and Lai [9]. The comparison of the LDOS at different Fe sites in figure 3(b) clearly shows why the FeIII atoms have the smallest spin magnetic moments. The FeIII LDOS has an increased band width and the smallest exchange splitting due to the hybridization interaction with N atoms. In contrast, FeI atoms have the largest spin magnetic moment because the exchange splitting of the LDOS is the largest.

Orbital polarizations of Fe atoms stemming from the spin–orbit interaction are non-negligible. Orbital magnetic moments of 0.07, 0.05, 0.05, and $0.07\mu_B$ are obtained for FeI, FeII, FeIII, and FeIV atoms, respectively. These values are a little larger than the value of the pure BCC Fe element, $0.03\mu_B$, but close to that of pure FCC Fe element, $0.06\mu_B$ [12]. These observations indicate that the local environment of each Fe atom in $Sm_2Fe_{17}N_3$ forming the stacking geometry is close to that of FCC Fe. In the case of the Sm atom, the

orbital magnetic moment, $-1.99\mu_B$, is polarized antiparallel to the spin magnetic moment. However, the magnitude of the orbital magnetic moment of the Sm atom determined in this way seems to be too small compared to the value of free trivalent Sm ions anticipated from Hund's rule, which is not well treated in our perturbation method.

Table 3 compares the calculated magnetic moments of $Sm_2Fe_{17}N_3$ with those of Sm_2Fe_{17}. We have also presented theoretical results for $Nd_2Fe_{17}N_3$ by Gu and Lai [9] and those for Y_2Fe_{17} by Coehoorn [18]. Compared to Sm_2Fe_{17}, the magnetic moment of the FeIII atom is reduced but those of the other Fe atoms are increased in $Sm_2Fe_{17}N_3$. This table shows that Sm_2Fe_{17} has the largest magnetic moment at the FeI site as in $Sm_2Fe_{17}N_3$, and the smallest magnetic moment at the FeII site. Such a trend is similar to the trend in Y_2Fe_{17}. The average magnetic moment per Fe atom in $Sm_2Fe_{17}N_3$ ($= 2.29\mu_B$) is larger than that in Sm_2Fe_{17} ($= 2.16\mu_B$) by $\sim 6\%$, even though there are hybridization effects in $Sm_2Fe_{17}N_3$, caused by the addition of N atoms. The enhancement originates from the more localized character of Fe 3d electrons due to an increased unit cell volume and so increased interatomic distances among Fe atoms.

Table 3. Magnetic moment (in μ_B) and the hyperfine field (in Tesla) of each atom in $Sm_2Fe_{17}N_3$; theoretical results for Sm_2Fe_{17}, $Nd_2Fe_{17}N_3$, from Gu and Lai [9], and Y_2Fe_{17} from Coehoorn [18]; experimental results from the hyperfine field of Mössbauer spectra for $Y_2Fe_{17}N_{3-\delta}$ from Qi *et al* [19] are also presented for comparison.

	R	FeI	FeII	FeIII	FeIV	N
$Sm_2Fe_{17}N_3$ (present work)	5.31	2.65	2.46	1.96	2.42	−0.04
Hyperfine field (present work for $Sm_2Fe_{17}N_3$)	—	43.2	46.3	35.7	42.3	—
Sm_2Fe_{17} (present work)	4.93	2.52	1.87	2.26	2.09	—
$Nd_2Fe_{17}N_3$ [9]	0.48	2.48	2.66	1.51	2.19	0.08
Y_2Fe_{17} [18]	−0.29	2.29	1.91	2.25	1.97	—
Hyperfine field [19] (for $Y_2Fe_{17}N_{3-\delta}$)	—	40.1	36.7	35.0	31.9	—

No experimental results are available yet on the local magnetic moment in $Sm_2Fe_{17}N_3$. Hence we have provided, in table 3, experimental results for the hyperfine fields that were obtained from Mössbauer measurements on $Y_2Fe_{17}N_{3-\delta}$ by Qi *et al* [19], although the structure of $Y_2Fe_{17}N_3$ is different from that of $Sm_2Fe_{17}N_3$. The trend in our calculated hyperfine fields for $Sm_2Fe_{17}N_3$ does not agree with that in experimental values for $Y_2Fe_{17}N_3$. The magnitude of the Mössbauer hyperfine fields in $Y_2Fe_{17}N_3$ decreases from FeI to FeII, FeIII, and FeIV. However, as Qi *et al* have mentioned, there can be some uncertainty in determining the magnetic moment from the Mössbauer hyperfine field due to core electron polarization and the effect of 4s electrons. Therefore, more experimental work, such as the polarized neutron experiment, is required in order to compare calculated local magnetic moments with experimental values.

3. 4f photoemission spectra of R_2Fe_{17} (R = Nd, Sm)

The photoemission measurements were performed using synchrotron radiation. The procedures for sample preparations and PES measurements are same as those described in [20]. The total instrumental resolution (FWHM; full width at half maximum) was about 0.3 eV for the PES spectra in this paper. Figure 4(a) and (b) shows the valence-band PES spectra (in dots) of polycrystalline samples of Nd_2Fe_{17} and Sm_2Fe_{17}, obtained at photon

energies $h\nu$ = 128 eV and $h\nu$ = 140 eV, respectively. The structures between E_F and ~ 4 eV below in both spectra are identified as mostly due to the Fe 3d emissions, as will be confirmed in figure 5(a). The photon energies for these two PES spectra correspond to the well known Fano maxima of the Nd and Sm 4f photoionization cross sections, respectively, where the 4f emissions are resonantly enhanced [21]. Thus the structures between −4 eV and −8 eV in Nd_2Fe_{17} are due to the trivalent Nd $4f^3 \rightarrow 4f^2$ transitions. Similarly, the structures between −4 eV and −12 eV in Sm_2Fe_{17} arise from the trivalent Sm 4f emissions, i.e., they are due to the $4f^5 \rightarrow 4f^4$ transitions.

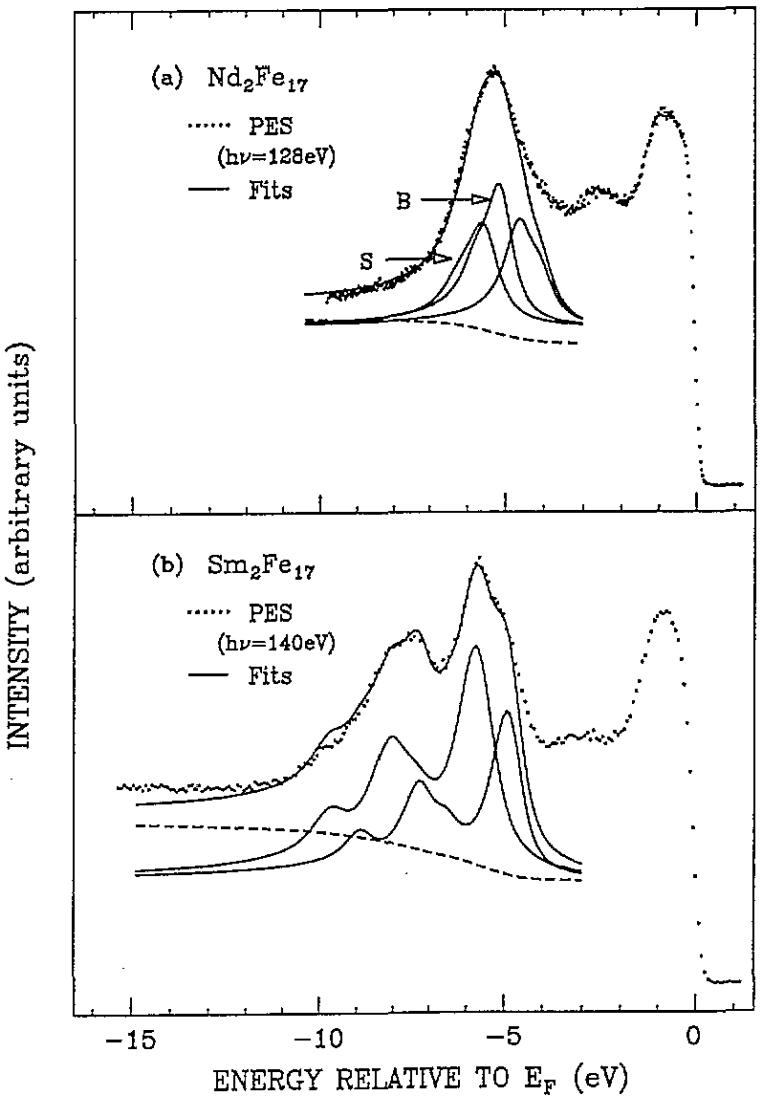

Figure 4. (a) Dots denote the valence-band photoemission (PES) spectrum of Nd_2Fe_{17}, taken at $h\nu$ = 128 eV. The full curves are the theoretical fits, which are obtained with $4f^3 \rightarrow 4f^2$ multiplet structures calculated as in [23]. (b) As (a) but for Sm_2Fe_{17}. Dots denote the valence-band PES spectrum, taken at $h\nu$ = 140 eV. The full curves are the theoretical fits, obtained by using the $4f^5 \rightarrow 4f^4$ multiplet structures.

We note that the line shapes of the Nd $4f^2$ and Sm $4f^4$ final-state peaks are much broader than those of pure elemental Nd and Sm metals [22]. In order to find the origin of the broad 4f PES line shapes, we have fitted the trivalent emission parts with the Nd $4f^2$ and Sm $4f^4$ final-state multiplet structures calculated from the coefficients-of-fractional-parentage analysis [23]. The final-state multiplets are assumed to have Doniach–Sunjic line shapes, to account for the Coulomb interaction between valence electrons and the 4f hole. The peaks are convolved with a Lorentzian to account for the finite lifetime of the 4f hole (2γ is the FWHM of the Lorentzian broadening). They are further convolved with a Gaussian to simulate the instrumental resolution. The results of a curve fitting are represented by full curves.

It is found that the Nd $4f^2$ PES peaks of Nd_2Fe_{17} (figure 4(a)) are fitted with three sets of components. The highest-binding-energy peaks, labelled 'S' (with the peak maximum at -5.62 eV), and the middle-binding-energy peaks, labelled 'B' (with the peak maximum at -5.15 eV), correspond to the *surface* and the *bulk* $4f^2$ final-state multiplets, as in the pure Nd metal, respectively. 2γ for the 'B' and 'S' components is 0.7 eV and 0.86 eV, respectively, which are close to the corresponding values for the pure Nd metal (0.76 eV and 1.0 eV, respectively) [22]. The intensity ratio of the two components, $I_B/I_S = 1.3 \pm 0.1$, is comparable to those values for the pure Nd metal (1.5 at $h\nu = 100$ eV). The energy separation between the two components is $\Delta = 0.47 \pm 0.05$ eV, which is also comparable to Δ for the Nd metal (~ 0.5 eV). However, besides *surface* and *bulk* peaks, another set of components (at -3.6 eV and -4.2 eV) is required to fit the experimental Nd 4f spectrum of Nd_2Fe_{17}. We interpret that these extra components reflect a transfer of the Nd 4f spectral weight toward E_F, which is caused by the hybridization between Nd 4f and Fe 3d states.

In figure 4(b), we present the results of fitting the Sm $4f^4$ PES spectrum of Sm_2Fe_{17} with two sets of peak components, both of which are assumed to correspond to the $4f^4$ configurations. The higher- and lower-binding-energy peaks are separated from each other by 0.83 ± 0.05 eV. The intensity ratio of the higher- and lower-binding-energy components is 1.6 ± 0.1. One might be tempted to assign the higher- and lower-binding-energy peaks as the *surface* and *bulk* $4f^4$ final-state multiplet structures, respectively. But such an interpretation is not plausible for the following reasons [24]. Under the above interpretation, the intensity of the *surface* peak is larger than that of the *bulk* peak, which is opposite to the behaviours observed in other rare-earth materials. The intensity ratio of the *bulk* to *surface* trivalent 4f peaks in the light rare-earth metals is $I_B/I_S \simeq 1.5$–2.0 for $h\nu \simeq 100$–200 eV [22]. Secondly, the binding energies of the *bulk* 4f peaks are too low, as compared to the pure Sm metal and Sm compounds. Finally, we have found that a comparable quality of fits can be obtained using some other set for the lower-binding-energy-peak components, for which the energy separations and their intensity ratios among the peaks are different from those of the $4f^4$ configurations. This suggests that it is rather fortuitous to obtain a good fit using the two sets of $4f^4$ configurations, shifted relative to each other.

It seems to be more reasonable to assign the lower-binding-energy peaks as the new 4f states which arise from the hybridization effect between Sm 4f and Fe 3d states. The higher-binding-energy peaks are assigned as the atomic-like *bulk* $4f^4$ multiplet structures, corresponding to the trivalent Sm 4f peaks in the pure Sm metal. Such an interpretation implies that there are no surface-shifted trivalent Sm 4f PES peaks in Sm_2Fe_{17}, and that the valence state of surface Sm atoms in Sm_2Fe_{17} is mostly divalent. The above assignment is consistent with that in Nd_2Fe_{17}, and we believe that these extra lowest-binding-energy peaks in the 4f PES spectra of Nd_2Fe_{17} and Sm_2Fe_{17} cause the line widths of the trivalent 4f PES emissions to be larger than those of pure Nd and Sm metals.

4. Comparison of the Fe 3d states

In figure 5, we compare the measured Fe 3d PES spectra with the calculated Fe 3d angular-momentum-projected local densities of states (PLDOSs) of R_2Fe_{17} (R = Nd, Sm), $Sm_2Fe_{17}N_3$, and $Nd_2Fe_{14}B$, in various ways. We show the PLDOS, obtained from both spin-unpolarized and spin-polarized calculations, corresponding to the paramagnetic and ferromagnetic phases, respectively. For the spin-polarized 3d PLDOS, the majority- and minority-spin PLDOSs are summed and averaged over sites. Then the regions of the results below E_F are taken and they are convolved with a Gaussian of 0.3 eV at FWHM to simulate the instrumental resolution.

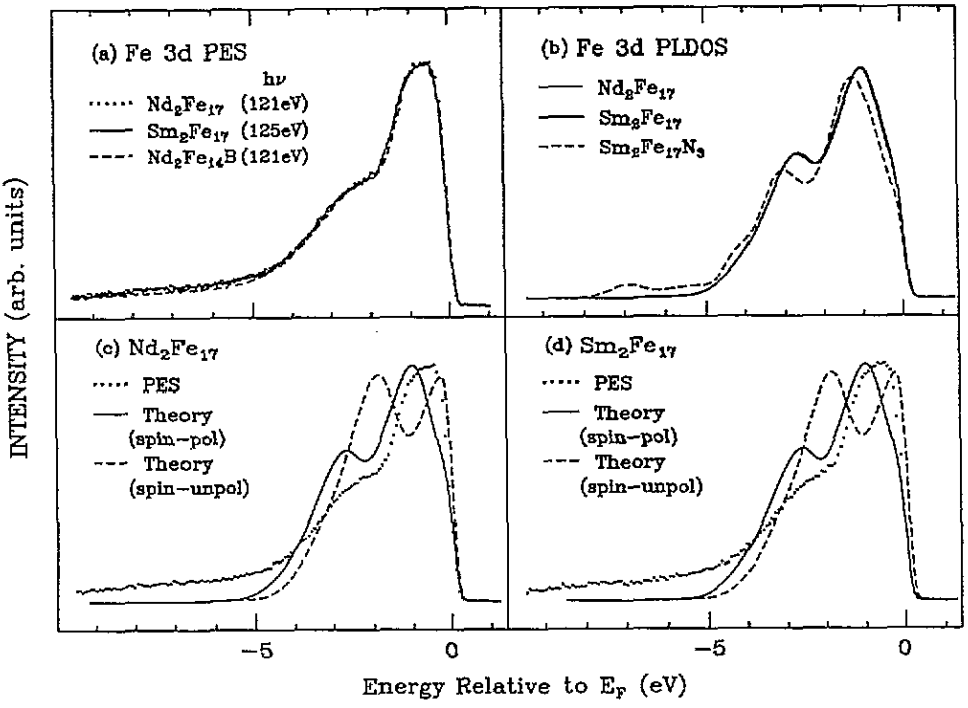

Figure 5. (a) Comparison of the valence-band PES spectra for Nd_2Fe_{17}, Sm_2Fe_{17}, and $Nd_2Fe_{14}B$, taken at $h\nu$ = 121 eV, 125 eV, and 121 eV, respectively. Note that they are essentially identical. (b) Comparison of the calculated Fe 3d PLDOSs for Nd_2Fe_{17}, Sm_2Fe_{17}, and $Sm_2Fe_{17}N_3$. Note the larger band width and the shifted peak positions in $Sm_2Fe_{17}N_3$. (c) Comparison of the $h\nu$ = 121 eV valence-band PES spectrum (in dots) with the calculated Fe 3d PLDOS for Nd_2Fe_{17}. The full and broken curves represent the calculated Fe 3d PLDOS for ferromagnetic and paramagnetic phases, respectively. (d) As (c) but for Sm_2Fe_{17}. Comparison of the $h\nu$ = 125 eV valence-band PES spectrum (in dots) with the calculated Fe 3d PLDOS for Sm_2Fe_{17}.

Figure 5(a) compares the valence-band PES spectra of Nd_2Fe_{17}, Sm_2Fe_{17}, and $Nd_2Fe_{14}B$, taken at $h\nu$ = 121 eV, 125 eV, and 121 eV, respectively. At these photon energies, Fe 3d emissions are dominant over emissions from other states, and so these spectra can be considered to represent the Fe 3d emissions. For the purpose of this study, it would be ideal to compare the Fe 3d PES spectra of Sm_2Fe_{17} and $Sm_2Fe_{17}N_3$. However, we do not have the PES data for $Sm_2Fe_{17}N_3$, because of difficulties in the preparation of an $Sm_2Fe_{17}N_3$

sample appropriate for the PES measurements. Instead, we present here the measured Fe 3d PES spectrum of $Nd_2Fe_{14}B$ [25] in order to show the effect of interstitial B atoms in the measured PES spectrum, which is expected to be similar to that of N atoms in $Sm_2Fe_{17}N_3$ [17].

This figure shows that the Fe 3d electronic structures are almost identical in Nd_2Fe_{17}, Sm_2Fe_{17}, and $Nd_2Fe_{14}B$, with the following common features. They are rather broad as compared to the rare-earth 4f spectra. No pronounced satellite structures are observed, suggesting that Coulomb interactions between Fe 3d electrons are smaller than Fe 3d band widths in these compounds. They exhibit two peak structures with a main peak at ~ -0.5 eV and a broad bump at ~ -2.5 eV. The two peaks are separated from each other by about 2 eV, which can be a measure of the exchange splitting for the Fe 3d bands (see figure 3(a)).

Figure 5(b) compares the theoretical Fe 3d PLDOS of Nd_2Fe_{17}, Sm_2Fe_{17}, and $Sm_2Fe_{17}N_3$, obtained from the spin-polarized calculations. In agreement with the measured Fe 3d PES spectra in (a), the calculated Fe 3d PLDOSs of Nd_2Fe_{17} and Sm_2Fe_{17} are essentially identical. Compared to Sm_2Fe_{17}, the site-averaged Fe 3d PLDOS of $Sm_2Fe_{17}N_3$ is shifted toward higher binding energies. In $Sm_2Fe_{17}N_3$, some of the Fe 3d spectral weight is transferred down to ~ -6—-8 eV, the occupied band width is larger, and the DOS at E_F is lower than that of Sm_2Fe_{17}. As we have pointed out from figure 3(b), such changes in the Fe 3d PLDOS of $Sm_2Fe_{17}N_3$ reflect the effect of the hybridization, mainly between FeIII atoms and N atoms.

Figure 5(c)and (d) compares the calculated PLDOS with the measured valence-band spectra for Nd_2Fe_{17} and Sm_2Fe_{17}, respectively. The PES spectra are the same as those shown in (a). In both parts of the figure, dots denote the measured PES spectra, and full and broken curves denote the spin-polarized and spin-unpolarized Fe 3d PLDOS, respectively. These comparisons for Nd_2Fe_{17} and Sm_2Fe_{17} show that the occupied band widths of the calculated Fe 3d PLDOS agree reasonably well with those of the measured Fe 3d PES spectra, suggesting that Fe 3d Coulomb correlation interaction energies are smaller than the Fe 3d band widths. The separation between the peak maximum and the bump at higher binding energy also agrees well between theory and experiment. However, some discrepancy is observed between experiment and theory in the peak positions. Neither spin-polarized nor spin-unpolarized peak positions in the Fe 3d PLDOS agree with the experimental peak positions, which in fact lie in between the peaks of the spin-polarized and spin-unpolarized Fe 3d PLDOS. A noticeable discrepancy is also observed in the weight distribution. Such a discrepancy could be partially due to matrix-element effects [26, 27], which are not included in the theory.

The deviation in the peak positions may be interpreted as due to the finite temperature at which the PES measurements were performed. Our PES measurements were performed below T_C, but at finite temperature, ~ 60 K. Since the exchange splitting is expected to increase as the temperature decreases below T_C, it is anticipated that the observed Fe 3d PES peaks will be located between the peaks of the paramagnetic and ferromagnetic Fe 3d PLDOS. This argument is supported by fact that, for both compounds, the Fe 3d PLDOSs for the ferromagnetic phase show better agreement with the measured Fe 3d PES spectra than those for the paramagnetic phase, considering that the PES spectra were obtained well below T_C. Temperature-dependent exchange splitting was indeed observed in the angle-resolved PES studies of Gd metal [28]. It should be noted, however, that the exchange splitting of ferromagnetic materials at finite temperatures is a controversial problem in itself [29].

On the other hand, we cannot exclude the possibility of the correlation effects among Fe 3d electrons accounting for the observed discrepancy in the peak positions between experiment and theory. It is well known that the LDA description of the electronic structures is not good for strongly correlated materials. The absence of satellite structures in the Fe 3d

PES spectra may indicate that correlation effects among Fe 3d electrons are not very large in these systems. To resolve this issue, more experimental data are required, such as the temperature dependence of the PES spectra and spin-polarized photoemission measurements.

5. Conclusions

From self-consistent LMTO band-structure calculations, it is found that N atoms substantially reduce the magnetic moments of neighbouring Fe atoms through the hybridization interaction and also play a role in stabilizing the crystal structure. The average magnetic moment of Fe atoms in the ferromagnetic phase of $Sm_2Fe_{17}N_3$ is estimated to be $2.29\mu_B$, which is $\sim 6\%$ larger than the magnetic moment of Sm_2Fe_{17}, $2.16\mu_B$. The FeI(6c) atoms, which are located farthest from N atoms and surrounded by 12 nearest-neighbour Fe atoms, have the largest magnetic moment ($2.65\mu_B$), while the FeIII(18f) atoms, whose hybridization interactions with N atoms are very strong, have the smallest magnetic moment ($1.96\mu_B$). The orbital magnetic moments of Fe atoms stemming from the spin–orbit interaction are estimated to be ~ 0.05–$0.07\mu_B$.

Photoemission measurements show that the *bulk* Nd and Sm atoms are nearly trivalent in Nd_2Fe_{17} and Sm_2Fe_{17}. The 4f PES line shapes are observed to be broader than in the pure Nd and Sm metals, which reflects the hybridization between Nd/Sm 4f and Fe 3d states. The measured Fe 3d PES spectra of Nd_2Fe_{17}, Sm_2Fe_{17}, and $Nd_2Fe_{14}B$ are found to be essentially the same in the the large-energy-scale structures. They are broad and do not exhibit pronounced satellite structures.

For Nd_2Fe_{17} and Sm_2Fe_{17}, the measured Fe 3d PES band widths are comparable to the calculated Fe 3d PLDOS widths below E_F. Nevertheless the experimental peak positions lie in between the peaks of paramagnetic and ferromagnetic Fe 3d PLDOSs. Such deviations in the peak positions can be ascribed to the finite-temperature effect of the PES measurements, although more detailed PES experimental information is required.

Acknowledgments

This work has been supported by the Korean Science and Engineering Foundation under contract number 921-0200-005-2 and by the Centre for Advanced Materials Physics at POSTECH. The experiment was performed at the Synchrotron Radiation Center (SRC) of the University of Wisconsin-Madison. Funds for travel to the SRC were provided by the Pohang Light Source.

References

[1] Coey J M D and Sun H 1991 *J. Magn. Magn. Mater.* **87** L251
Sun H, Coey J M D, Otani Y and Hurley D P F 1990 *J. Phys.: Condens. Matter* **2** 6465
Coey J M D and Otani Y 1991 *Magn. Soc. Japan* **15** 677

[2] Wohlfarth E P and Buschow K H J 1988 *A Handbook on the Properties of Magnetically Ordered Substances* vol 4 (Amsterdam: North-Holland)

[3] Burzo E and Kirchmayr H R 1989 *Handbook on the Physics and Chemistry of Rare Earths* vol 12, ed K A Gshneidner and L Eyring (Amsterdam: North-Holland) ch 82

[4] Herbst J H 1991 *Rev. Mod. Phys.* **63** 819

[5] Coey J M D 1991 *Phys. Scr.* T **39** 21

[6] Woods J P, Fernando A S, Patterson B M, Welipitiya D, Jaswal S S and Sellmyer D 1991 *Proc. 25th SRC User Group Meeting*
[7] Jaswal S S, Yelon W B, Hadjipanayis G C, Wang Y Z and Sellmyer D J 1992 *Phys. Rev. Lett.* **67** 644
[8] Andersen O K 1975 *Phys. Rev.* B **12** 3060
Skriver H L 1984 *The LMTO Method (Springer Ser. Solid State Sci. 41)* (Berlin: Springer).
[9] Gu Z and Lai W 1992 *J. Appl. Phys.* **71** 3911
[10] Hohenberg P and Kohn W 1964 *Phys. Rev.* **136B** 864
Kohn W and Sham L J 1965 *Phys. Rev.* **140** A1133
[11] Wood C, Min B I, Benedek R and Garner J 1989 *Phys. Rev.* B **39** 4853
[12] Min B I and Jang Y-R 1991 *J. Phys.: Condens. Matter* **3** 5131
[13] Srivastava G P 1984 *J. Phys. A: Math. Gen.* **17** L317
[14] Richter M and Eschrig H 1991 *Physica* B **172** 85
Brooks M S S, Nordström L and Johansson B 1991 *Physica* B **172** 95
[15] Freeman A J, Min B I and Norman M R 1987 *Handbook on the Physics and Chemistry of Rare Earths* vol 10, ed K A Gshneidner, L Eyring and S Hüfner (Amsterdam: Elsevier) pp 165–229
[16] Min B I unpublished
[17] Min B I, Jeong J H and Yang C J 1992 *J. Korean Magn. Soc.* **2** 193
[18] Coehoorn R 1989 *Phys. Rev.* B **39** 13072
[19] Qi Q, Sun H, Skomski R and Coey J M D 1992 *Phys. Rev.* B **45** 12278
[20] Kang J-S, Hong J H, Jeong J I, Choi S D, Yang C J, Lee Y P, Olson C G, Min B I and Allen J W 1992 *Phys. Rev.* B **46** 15689
[21] Fano U 1961 *Phys. Rev.* **124** 1866
[22] Gerken F, Flodstrom A S, Barth J, Johansson L I and Kunz C 1985 *Phys. Scr.* **32** 43
[23] Gerken F 1983 *J. Phys. F: Met. Phys.* **13** 703
[24] As the sample ages, no differences are observed in behaviour for the two sets of peaks, suggesting that they have similar bulk and/or surface characters.
[25] Kang J-S to be published
[26] Speier W, Fuggle J C, Durham P, Zeller R and Traum M M 1988 *J. Phys. C: Solid State Phys.* **21** 2621
[27] Nahm T-U, Han M, Oh S-J, Park J-H, Allen J W and Chung S-M 1993 *Phys. Rev. Lett.* **70** 3663
[28] Kim B, Andrew A B, Erskine J L, Kim K and Harmon B N 1992 *Phys. Rev. Lett.* **68** 1931
[29] Kisker E and Carbone C 1990 *Proc. Int. School Phys. 'Enrico Fermi'* course 108, ed M Campagna and R Rosei (Amsterdam: North-Holland) p 401 and references therein